Research Square

Preprints are preliminary reports that have not undergone peer review.
They should not be considered conclusive, used to inform clinical practice,
or referenced by the media as validated information.

Nanoparticle Superlattices with Non-Equilibrium Crystal Shapes

Robert Macfarlane

rmacfarl@mit.edu

Massachusetts Institute of Technology https://orcid.org/0000-0001-9449-2680

Matthew Ye

Massachusetts Institute of Technology

Theodore Hueckel

Massachusetts Institute of Technology

Perapat Gatenil

MIT

Keisuke Nagao

MIT

W Carter

M.I.T. https://orcid.org/0000-0001-7564-7173

Article

Keywords:

Posted Date: January 18th, 2024

DOI: https://doi.org/10.21203/rs.3.rs-3612421/v1

License: This work is licensed under a Creative Commons Attribution 4.0 International License.
Read Full License

Additional Declarations: There is **NO** Competing Interest.

Nanoparticle Superlattices with Non-Equilibrium Crystal Shapes

Matthew Ye, Theodore Hueckel, Perapat P. Gatenil, Keisuke Nagao, W. Craig Carter, Robert J. Macfarlane[†]

Department of Materials Science and Engineering, Massachusetts Institute of Technology, 77 Massachusetts Avenue, Cambridge MA 02139, USA

[†] Address correspondence to rmacfarl@mit.edu

Abstract

Nanoparticle assembly is a materials synthesis strategy that enables precise control of nanoscale structural features. Concepts from traditional crystal growth research have been tremendously useful in predicting and programming the unit cell symmetries of these assemblies, as their thermodynamically favored structures are often identical to atomic crystal analogues. However, these analogies have not yielded similar levels of influence in programming crystallite shapes, which are a consequence of both the thermodynamics and kinetics of crystal growth. Here we demonstrate kinetic control of colloidal crystal shape using nanoparticle building blocks that rapidly assemble over a broad range of concentrations, thereby producing well-defined crystal habits with symmetrically oriented dendritic protrusions and providing insight into the crystals' morphological evolution. Counterintuitively, these non-equilibrium crystal shapes actually become more common for colloidal crystals synthesized closer to equilibrium growth conditions.

This deviation from typical crystal growth processes observed in atomic or molecular crystals is shown to be a function of the drastically different timescales of atomic and colloidal mass transport, and thus this work provides design principles to expand the morphological diversity of nanoparticle superlattice crystal habits beyond the anhedral or equilibrium polyhedral shapes synthesized to date. Finally, we use this insight to synthesize crystallite shapes that have never before been observed, demonstrating the ability to both predict and program kinetically-controlled superlattice morphologies.

Introduction

The synthesis of ordered superlattices from a metastable colloidal dispersion is easily analogized to the growth of atomic or molecular crystals from a supersaturated solution or vapor, since the products of both processes tend to exhibit similar unit cell symmetries and crystal habits[1–8]. For example, both atomic[9] and colloidal crystals with CsCl unit cells[4,5,10–13] tend to form rhombic dodecahedral crystallites. This geometry is the Wulff shape for both crystal types, as it is enclosed by CsCl's lowest energy {110} planes, and the Gibbs-Wulff theorem that predicts these crystals' equilibrium shapes is indifferent to the sizes of their constituent building blocks[14]. However, while strong analogies exist for the synthesis of thermodynamically favored crystal habits using multiple sizes of colloidal building blocks, atomic and molecular solids exhibit a significantly greater diversity of kinetic morphologies, including dendritic, needlelike, plate-shaped, hollow, or hopper-shaped crystals[15,16]. In contrast, nanoparticle assembly has only produced a few examples of kinetically controlled but still well-defined crystal habits[17,18], and most colloidal crystals

assembled under far-from-equilibrium conditions do not have any consistent shape at all, often forming anhedral or polycrystalline agglomerates[7].

The reason for this difference could be that even though both types of thermoreversible crystal formation are affected by similar variables (e.g. precursor concentration, temperature)[2,6,7,10], the accessible ranges of these variables differ significantly for atomic and colloidal systems. For instance, when compared to their atomic counterparts, colloidal crystals have slower particle rearrangement kinetics relative to the rate of new particle addition to the crystallite surface[19]. As a result, the synthesis of single-crystal colloidal superlattices with well-defined habits has typically required extremely gradual transitions through the solidification temperature, necessitating long crystallization timescales. Moreover, colloidal building blocks with highly addressable bonding interactions tend to be synthesized in small quantities, restricting most assembly methodologies to low particle concentrations. Thus, we hypothesized that the limited number of observed kinetic shapes in nanoparticle assembly may be a consequence of our inability to reliably access regimes in which growth is simultaneously slow enough to achieve crystallinity yet fast enough to generate metastable crystal habits.

To test this hypothesis, it is necessary to assemble crystals from nanoscale building blocks that push the boundaries of accessible concentrations and crystallization timescales. Nanocomposite tectons (NCTs) are an ideal building block for such investigations, as they consist of an inorganic nanoparticle core decorated with a dense brush of synthetic polymers, and particle assembly is driven by dynamic bonding interactions between polymer chain end groups[10,20,21]. Because the polymeric ligands can be synthesized on a gram scale, high-concentration assembly is more feasible with NCTs than comparable alternatives. Additionally, the dynamic supramolecular bonds

enable facile particle rearrangement, allowing crystalline structures to be achieved at cooling rates 100 times faster than other enthalpically-driven assembly systems[2,4,7,10,22].

Results & Discussion

Assembly Conditions for Non-Equilibrium Morphologies

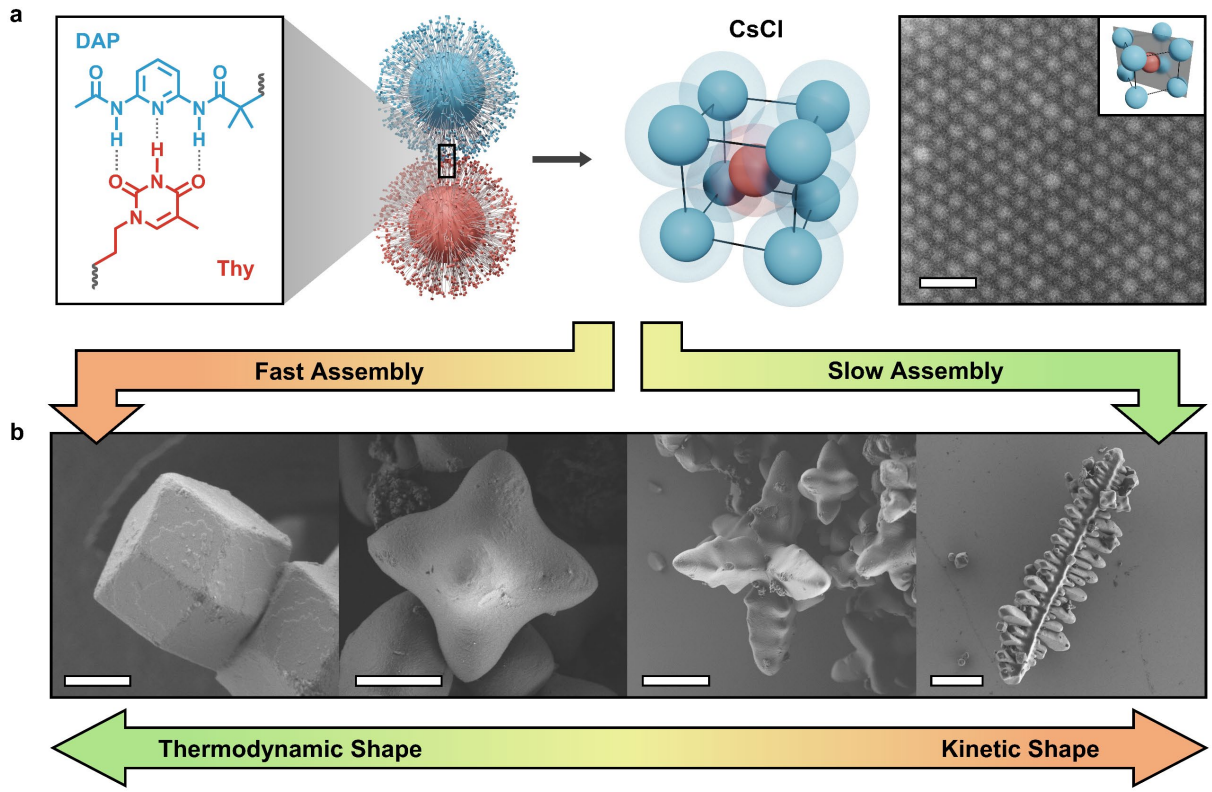

Fig. 1 | Morphological diversity of CsCl superlattices assembled from complementary NCTs. a, Nanoparticles functionalized with DAP- and Thy-terminated polymers assemble into CsCl superlattices. The SEM image shows the [110] surface of a CsCl-type NCT crystallite. **b**, NCT crystallite shape varies with cooling rate following a counterintuitive trend. At fast cooling rates, they exclusively form the Wulff shape (rhombic dodecahedra), but form increasingly anisotropic and dendritic shapes when assembled more slowly (hexapods at intermediate rates, and columnar dendrites at the slowest cooling rates). Scale bars: 50 nm (**a**); 2, 5, 15, and 30 μm (**b**, left to right).

To explore how assembly kinetics affect crystallite morphology, binary sets of complementary NCTs were synthesized. The majority of the work presented here used 8 nm iron oxide cores and 13 kDa polystyrene chains (see Supplementary Information for full details of all systems). The

polymer chains on each NCT terminated in either diaminopyridine (DAP) or thymine (Thy) end-groups (Fig. 1a); NCTs were assembled into CsCl superlattices by cooling equimolar mixtures of DAP- and Thy-NCTs at a fixed starting concentration (640 nM) but varied ramp rates (0.4, 0.2, 0.1, or 0.025 °C/min). The resulting crystallites were analyzed with scanning electron microscopy (SEM) and small-angle X-ray scattering (SAXS) to determine their morphology and crystal structure.

Surprisingly, while all assembly conditions produced discrete single crystals, the crystal habits exhibited the exact opposite trend of what would be expected from traditional crystal growth (Fig. 1b). NCTs cooled at the fastest rate (0.4 °C/min) formed sharply-faceted rhombic dodecahedra, the thermodynamically favored crystallite shape. Conversely, at slower cooling rates (which would typically favor thermodynamic structures), NCTs formed hexapod-shaped crystallites with perpendicular protrusions. At the slowest cooling rate, they even formed large columnar dendrites, a morphology commonly associated with kinetic growth (Figs. 1b, 2a, Supplementary Figs. 5-8). Despite these differences in crystallite shape, all structures appeared to be single-crystalline based on their consistent cubic symmetry. Moreover, SAXS analysis showed that all assembly conditions formed CsCl crystals of identical quality (Fig. 2b), indicating that this morphological trend is not correlated with any variation in the underlying crystal structure. We would note that, even though they formed under slower cooling rates, it is unlikely that hexapods or columnar dendrites represent a thermodynamically optimal crystal shape, as they have significantly more unfavorable exposed surface area than a compact rhombic dodecahedron of equal volume. These results indicate that, contrary to our intuition of conventional solidification processes, *faster* cooling favors equilibrium structures while *slower* cooling favors non-equilibrium structures.

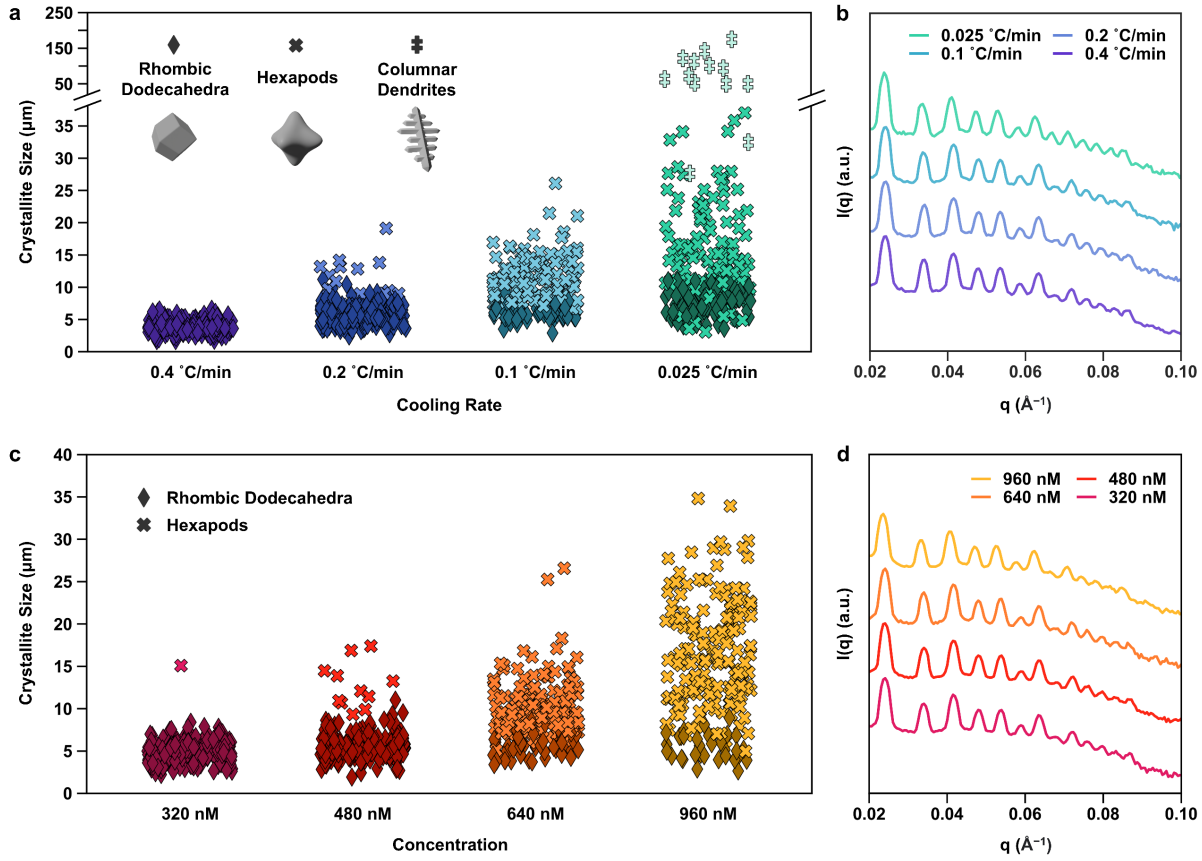

Fig. 2 | Cooling rate and concentration effects on crystal habit. a-d, Shape and size distributions (**a**, **c**) and SAXS data (**b**, **d**) for NCT crystallites assembled at fixed concentration (640 nM) with varying cooling rates (**a**, **b**), and at fixed cooling rate with varying concentrations (**c**, **d**).

To better understand this counterintuitive result, it was necessary to deconvolute the multiple effects of altering cooling rate on crystal growth. While more gradual cooling provides longer time windows for particle reconfiguration (which should favor the thermodynamically preferred crystal habit), it also promotes the formation of larger crystallites (Fig. 2a). We therefore hypothesized that the emergence of dendritic structures was directly enabled by the increase in crystallite size, and only indirectly correlated with slower cooling. Since crystallite size is also known to increase with concentration[10], we tested this hypothesis by assembling batches of the same NCTs described above using a fixed cooling rate (0.1 °C/min) but varied concentrations (320, 480, 640, or 960 nM). While NCTs assembled at the lowest concentration formed almost exclusively rhombic

dodecahedra, higher NCT concentrations correlated with increasing hexapod character, meaning both a higher fraction of hexapod-shaped crystallites, and each individual hexapod in a batch having more protruding arms (Fig. 2c, Supplementary Figs. 7, 9-11). All growth conditions were again observed to produce CsCl lattices, with uniform crystal quality across this concentration range (Fig. 2d).

Shape Evolution Mechanism

To further confirm the correlation between crystal size and hexapod character, a sample of NCTs (640 nM, 0.1 °C/min cooling rate) was fractionated using a density gradient column. Fractions with smaller crystallites contained exclusively rhombic dodecahedra, while fractions with larger crystallites contained almost exclusively hexapods (Fig. 3a-c). From these observations, we propose that NCTs initially crystallize in a manner consistent with their predicted Wulff shape. However, once the crystals reach a critical size, polyhedral growth ceases to be stable and their continued growth proceeds dendritically, leading to a gradual transformation into a hexapodal morphology. This shape evolution pathway can be understood by observing that CsCl rhombic dodecahedra have six 4-fold ⟨100⟩-oriented vertices and eight 3-fold ⟨111⟩-oriented vertices; the hexapod structure is consistent with selective growth outward from the most exposed ⟨100⟩ vertices (Fig. 3d, Supplementary Fig. 17). This pathway can be confirmed empirically by examining SEM images of crystallites whose growth stopped mid-transformation due to the depletion of the feedstock (Fig. 3e). While all vertices are still visible in this arrested crystal, the protrusion of the 4-fold vertices is significantly more pronounced.

The appearance of concave features at the facet centers (Fig. 3e) points to a mechanism of polyhedral instability similar to snowflakes growing from a supersaturated vapor[15]. Because colloidal building blocks have a drastically lower diffusivity than atoms, their assembly can be

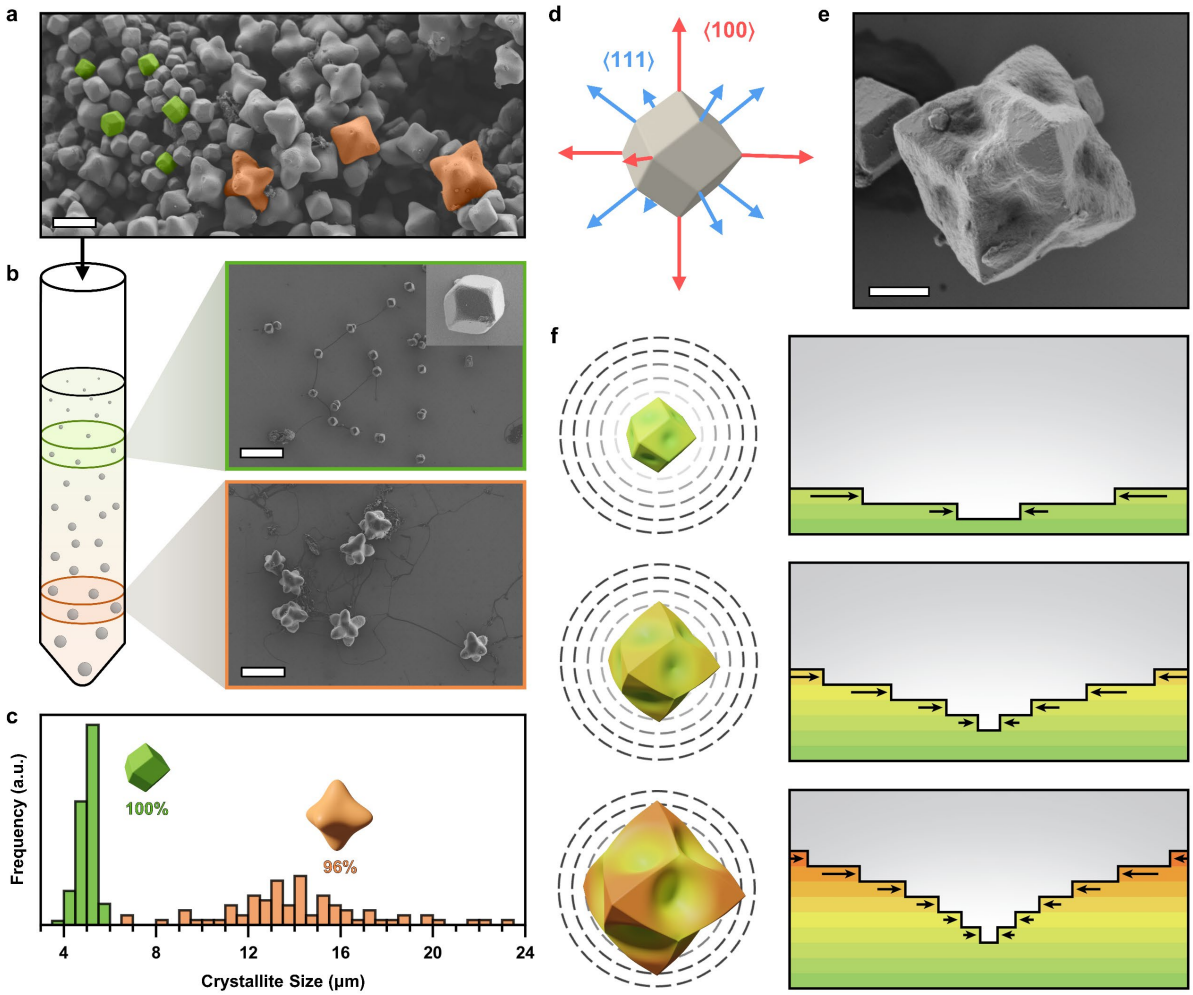

Fig. 3 | Shape evolution of NCT crystallites. a, NCTs assembled at 640 nM with a 0.1 °C/min cooling rate form a mixture of rhombic dodecahedra (green) and hexapods (orange). **b**, **c**, After fractionation in a density-gradient column, SEM images of NCT crystallites in each fraction (**b**) and size distribution histograms (**c**) show the segregation of rhombic dodecahedra and hexapods, suggesting shape evolution during growth. **d**, CsCl rhombic dodecahedra have six 4-fold ⟨100⟩-oriented vertices (red arrows) and eight 3-fold ⟨111⟩-oriented vertices (blue arrows). **e**, Partially transformed crystallites exhibit concavity at the facet centers, indicating that initial rhombic dodecahedra gradually transform via faster growth from the ⟨100⟩-oriented axes. **f**, Facet curvature arises because crystallite growth occurs non-uniformly across its surface. Inhomogeneous supersaturation (which favors corner growth) occurs due to the protrusion of corners into the surrounding growth medium. However, as these corners grow, the surface begins to exhibit nonuniform step density, which favors the growth of facet centers. The balance of these factors leads to the observed concave curvature. Scale bars: 10 μm (**a**), 20 μm (**b**), 2 μm (**e**).

diffusion-limited even at slow cooling rates[23]. When a polyhedral crystal's growth is limited by the rate at which new particles approach the interface, a spherically-symmetric concentration gradient develops around it, causing an inhomogeneous local supersaturation across its surface[24].

As a result, new crystal layers preferentially nucleate near the most extended corners where the supersaturation is highest. As these new layers grow laterally outward away from the corners, their rate of expansion slows down with the decreasing supersaturation, resulting in an accumulation of surface steps at the facet centers where the supersaturation is lowest (Fig. 3f).

In the early stages of crystal growth, the predicted Wulff shape (i.e. the rhombic dodecahedron) persists because the rates of particle addition to facets and corners are counterbalanced by two competing factors that keep the growth rate isotropic enough to maintain the rhombic dodecahedral habit. Specifically, at the corners, the higher local particle concentration increases the number of particles approaching the surface, while at the facet centers, the higher step density increases the probability of particle attachment upon collision. These competing factors lead the facets to develop a concave topography, as a balance is struck between nucleating new layers at corners, and growing existing layers via attachment to steps at the facet centers. For small crystallites, the difference in local supersaturation between the corners and faces is small, so only a slight concavity emerges. As the crystal grows, the supersaturation becomes more inhomogeneous, so this balance is only maintained if the step density becomes increasingly nonuniform and the facets increasingly concave. At a critical size, however, the step density at the facet centers reaches a maximum, and this compensation mechanism breaks down[15,25,26]. The resulting overgrowth of the corners causes them to protrude into the surrounding concentration gradient, which further accelerates their growth through a Mullins-Sekerka-type positive feedback loop[27,28]. The selective extension of the 4-fold vertices over the 3-fold vertices can be attributed to differences in the extent of their protrusion, and is likely reinforced by the anisotropy of the rhombic dodecahedron's facets (Supplementary Discussion).

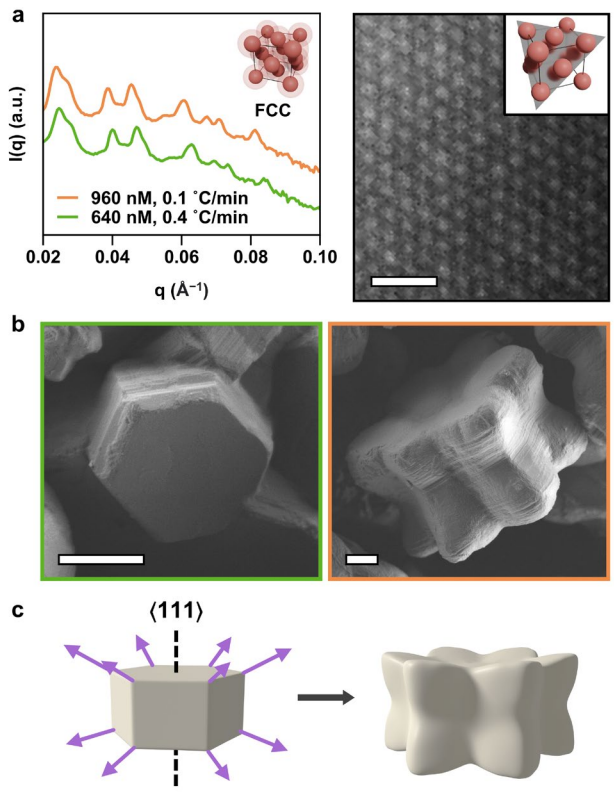

Fig. 4 | Dendritic growth of FCC superlattices. **a**, FCC superlattices can be assembled by inducing self-complementary interactions between Thy-NCTs. SAXS data shows FCC symmetry in growth conditions that favor convex and concave habits. SEM images show the presence of {111} planes on the surfaces of the crystallites. **b**, FCC crystals can form hexagonal prisms (left), which evolve into dodecapods with 6-fold rotational symmetry (right). **c**, The outward protrusion of all 12 vertices of the hexagonal prism results in the dodecapod morphology. Scale bars: 50 nm (**a**), 2 μm (**b**).

Dendritic Orientation Selection

One key feature of this growth mechanism is that dendritic orientation selection is determined by the geometry of the initial polyhedral crystal. This is in contrast to, for example, the growth of alloy dendrites from a supercooled melt, where dendrite orientation is determined by the crystallographic symmetry of the lattice[29]. In other words, we hypothesized that the six arms of these hexapods point along ⟨100⟩ directions because those vectors coincide with the locations of the 4-fold vertices on a rhombic dodecahedron, not because some anisotropic property such as surface tension has local extrema in the ⟨100⟩ directions. However, it is not possible to distinguish between these effects in CsCl superlattices, in which both the crystal habit and the unit cell have cubic symmetry.

While CsCl-type crystals cannot test the hypothesis that NCT crystallite shape dictates growth modes, it was recently demonstrated that NCTs can also be assembled into FCC superlattices by using melamine to mediate self-complementary interparticle bonding between Thy-NCTs[30]. FCC crystallites tend to form a variety of polyhedral shapes, including hexagonal prisms and

pentatwinned structures[4,30]. Thus, we predicted that FCC superlattices could be induced to adopt dendritic morphologies that lack cubic symmetry, thereby confirming the hypothesized effect of crystallite geometry on dendrite orientation. FCC NCT superlattices were assembled under conditions that favored convex habits (640 nM, 0.4 °C/min) and concave habits (960 nM, 0.1 °C/min) in the CsCl crystals; FCC crystal quality was identical for these conditions as confirmed by SAXS (Fig. 4a). While the former assembly condition yielded the expected mixture of faceted crystal habits, the latter yielded larger crystallites with a previously unobserved shape—dodecapods with 6-fold symmetry (Fig. 4b, Supplementary Figs. 12, 13, 15). This dodecapod morphology is consistent with our hypothesis, as it is the expected shape from overgrowth of all 12 corners of a hexagonal prism (Fig. 4c), and lacks cubic symmetry despite having a cubic unit cell. If dendritic orientation selection were governed by surface stiffness anisotropy (or any parameter that is a function of crystallographic vector), the multipod structure would be expected to have the same cubic symmetry as the superlattice. Additionally, dendritic morphologies corresponding to pentatwinned crystallites were not observed, possibly due to their lower degree of anisotropy (and thus smaller differences in supersaturation across their surface). These findings indicate that dendrite orientation is indeed dictated by crystallite shape and not by crystallographic direction-based anisotropic growth.

Conclusion

In this work, we have demonstrated that NCTs can crystallize into non-equilibrium morphologies, including hexapods, columnar dendrites, and dodecapods. Importantly, the morphological evolution of NCT crystals follows counterintuitive trends due to polyhedral instability, in which a competition between inhomogeneous supersaturation and nonuniform step density leads a subset

of vertices to protrude outward after the crystal reaches a sufficient size. This mechanism permits the synthesis of dendritic habits that do not conform to the crystallographic symmetry of the superlattice. These results are illuminating with regard to microstructural development in colloidal crystallization, a subject in which mechanistic understanding remains underdeveloped. While colloidal assembly methods already enable extremely precise control at the level of unit cell symmetry, understanding how to design microstructural features in these systems is crucial to fully dictating the properties of self-assembled materials and their incorporation into different technological applications[23,31,32]. Thus, the fundamental insight gained from these investigations enables the synthesis of future nanoparticle-based materials via both thermodynamic and kinetic control of multiple levels of structural hierarchy.

Methods

Iron Oxide Nanoparticle Synthesis

Iron oxide nanoparticles were synthesized via thermal decomposition of an iron oleate precursor according to previously reported procedures[33]. Iron oleate was synthesized by combining 7.8 g of iron(III) chloride hexahydrate, 27.2 g of sodium oleate, 60 mL of ethanol, 45 mL of water, and 105 mL of hexanes in a round-bottom flask and heating to 70 °C for 4 hours. The product was washed 3 times with water, dried by rotary evaporation, and further dried on a Schlenk line at 120 °C. Next, iron oleate, oleic acid, and either 1-octadecene or docosane (reagent quantities and solvent choice depend on targeted particle size) were combined in 3-neck flask, heated to 100 °C under vacuum to ensure dryness. The reaction vessel was evacuated and refilled with nitrogen 3 times, then heated with a ramp rate of 6 °C/min to reflux for 1 hour. After reacting, the mixture was transferred to a separate container and stored at 4 °C as a solid. Additional synthetic details are provided in the Supplementary Methods.

Polymer Synthesis

Polystyrene chains modified on one end with a DAP or Thy group and on the other end with a phosphonic acid group were prepared according to previously reported procedures[21]. Briefly, DAP- and Thy-initiators were first synthesized, and atom transfer radical polymerization was used to grow polystyrene chains from these initiators. Phosphonic acid groups were installed on the opposite terminus attachment of a propargyl phosphonate anchor via azide-alkyne cycloaddition. Complete synthetic protocols are available in the Supplementary Methods.

Nanoparticle Functionalization and Assembly

Iron oxide NCTs were prepared by combining iron oxide nanoparticles and phosphonic acid-terminated polymers in THF and gently mixing overnight at 25 °C to allow the polymer chains to graft to the nanoparticle surface. NCTs were washed several times by centrifugation in THF and toluene before final resuspension in toluene prior to assembly. CsCl-type and FCC superlattices were assembled by preparing, respectively, 1:1 mixtures of DAP- and Thy-NCTs and 300:1 mixtures of melamine and Thy-NCTs (with NCT concentrations determined by ICP-OES and UV-Vis spectroscopy) and cooling at a controlled rate in a thermal cycler from 65 °C to 25 °C. For SAXS analysis, the resulting NCT crystallites were added to polyimide capillaries and sealed with epoxy. For SEM imaging, the crystallites were gradually collapsed by incremental replacement of the toluene supernatant with a decane, then dried by allowing the decane to evaporate.

Size-Selective Purification of Assembled Crystallites

Dried NCT crystallites were sonicated in 300 μL of aqueous F-127 solution (0.2% w/v) for 30 minutes to ensure that individual crystallites remained separated during subsequent purification steps. After overnight sedimentation, the supernatant was replaced with 100 μL of the same F-127 solution for transfer to a density gradient column. The column was prepared by gently adding 2 mL of NaCl solutions of decreasing concentration (6.0 M, 5.4 M, 4.8 M, 4.2 M, and 3.6 M) to a centrifuge tube. After 150 minutes of sedimentation, 0.5 mL fractions were collected and washed by centrifuging at 12 *g* for 15 minutes and replacing with deionized water 3 times.

Data Availability. The data supporting the findings of this study are provided within the article or its Supplementary Information. Further data are available from the corresponding author upon request.

Supplementary Information. Detailed experimental procedures, including nanoparticle synthesis, polymer synthesis, nanoparticle functionalization, assembly, and characterization techniques are available in Supplementary Methods. Additional discussion on the contribution of anisotropic diffusion to dendritic orientation selection is available in Supplementary Discussion. Additional SEM images and experiments are included in Supplementary Notes 1 and 2, respectively.

Author Contributions. Experiments were designed by M.Y., T.H., and R.J.M. Experiments were conducted by M.Y., T.H., P.P.G., and K.N. Data analysis was performed by M.Y. All authors contributed to writing the manuscript.

Competing Interests. The authors declare no competing interests.

Acknowledgments. This work was supported by the Office of Naval Research (N00014-22-1-2148), and the Army Research Office (W911NF-18-1-0197), and made use of MRSEC Shared Experimental Facilities at MIT, supported by the NSF under award DMR 14-19807. The authors thank Margaret S. Lee for the production of iron oxide nanoparticles and Peter J. Santos for the production of polymers used in this work.

References

1. Shevchenko, E. V., Talapin, D. V., Kotov, N. A., O'Brien, S. & Murray, C. B. Structural diversity in binary nanoparticle superlattices. *Nature* **439**, 55–59 (2006).

2. Macfarlane, R. J. *et al.* Nanoparticle Superlattice Engineering with DNA. *Science* **334**, 204–208 (2011).

3. Gabrys, P. A., Zornberg, L. Z. & Macfarlane, R. J. Programmable Atom Equivalents: Atomic Crystallization as a Framework for Synthesizing Nanoparticle Superlattices. *Small* **15**, 1805424 (2019).

4. Auyeung, E. *et al.* DNA-mediated nanoparticle crystallization into Wulff polyhedra. *Nature* **505**, 73–77 (2014).

5. Kang, Y. *et al.* Heterogeneous Catalysts Need Not Be so "Heterogeneous": Monodisperse Pt Nanocrystals by Combining Shape-Controlled Synthesis and Purification by Colloidal Recrystallization. *J. Am. Chem. Soc.* **135**, 2741–2747 (2013).

6. Lewis, D. J., Zornberg, L. Z., Carter, D. J. D. & Macfarlane, R. J. Single-crystal Winterbottom constructions of nanoparticle superlattices. *Nat. Mater.* **19**, 719–724 (2020).

7. Boles, M. A., Engel, M. & Talapin, D. V. Self-Assembly of Colloidal Nanocrystals: From Intricate Structures to Functional Materials. *Chem. Rev.* **116**, 11220–11289 (2016).

8. Lee, M. S., Yee, D. W., Ye, M. & Macfarlane, R. J. Nanoparticle Assembly as a Materials Development Tool. *J. Am. Chem. Soc.* **144**, 3330–3346 (2022).

9. Uyeda, R. The morphology of fine metal crystallites. *Journal of Crystal Growth* **24–25**, 69–75 (1974).

10. Santos, P. J., Gabrys, P. A., Zornberg, L. Z., Lee, M. S. & Macfarlane, R. J. Macroscopic materials assembled from nanoparticle superlattices. *Nature* **591**, 586–591 (2021).

11. Hueckel, T., Hocky, G. M., Palacci, J. & Sacanna, S. Ionic solids from common colloids. *Nature* **580**, 487–490 (2020).

12. Wang, Y. *et al.* DNA origami single crystals with Wulff shapes. *Nat. Commun.* **12**, 3011 (2021).

13. Li, Z. *et al.* Accurate computational design of three-dimensional protein crystals. *Nat. Mater.* **22**, 1556–1563 (2023).

14. Ringe, E., Van Duyne, R. P. & Marks, L. D. Kinetic and Thermodynamic Modified Wulff Constructions for Twinned Nanoparticles. *J. Phys. Chem. C* **117**, 15859–15870 (2013).

15. Libbrecht, K. *Snow crystals: a case study in spontaneous structure formation*. (Princeton University Press, 2022).

16. Perkins, D. *Mineralogy*. (Pearson, 2014).

17. Seo, S. E., Girard, M., Olvera De La Cruz, M. & Mirkin, C. A. Non-equilibrium anisotropic colloidal single crystal growth with DNA. *Nat. Commun.* **9**, 4558 (2018).

18. Liao, C.-W., Lin, Y.-S., Chanda, K., Song, Y.-F. & Huang, M. H. Formation of Diverse Supercrystals from Self-Assembly of a Variety of Polyhedral Gold Nanocrystals. *J. Am. Chem. Soc.* **135**, 2684–2693 (2013).

19. Macfarlane, R. J. *et al.* Importance of the DNA "bond" in programmable nanoparticle crystallization. *Proc. Natl. Acad. Sci. U.S.A.* **111**, 14995–15000 (2014).

20. Zhang, J. *et al.* Self-Assembling Nanocomposite Tectons. *J. Am. Chem. Soc.* **138**, 16228–16231 (2016).

21. Santos, P. J. & Macfarlane, R. J. Reinforcing Supramolecular Bonding with Magnetic Dipole Interactions to Assemble Dynamic Nanoparticle Superlattices. *J. Am. Chem. Soc.* **142**, 1170–1174 (2020).

22. Santos, P. J., Cao, Z., Zhang, J., Alexander-Katz, A. & Macfarlane, R. J. Dictating Nanoparticle Assembly via Systems-Level Control of Molecular Multivalency. *J. Am. Chem. Soc.* **141**, 14624–14632 (2019).

23. Hueckel, T., Lewis, D. J., Mertiri, A., Carter, D. J. D. & Macfarlane, R. J. Controlling Colloidal Crystal Nucleation and Growth with Photolithographically Defined Templates. *ACS Nano* **17**, 22121–22128 (2023).

24. Berg, W. F. Crystal growth from solutions. *Proc. R. Soc. A* **164**, 79–95 (1938).

25. Chernov, A. A. Stability of faceted shapes. *J. Cryst. Growth.* **24–25**, 11–31 (1974).

26. Nanev, C. N. Instability of Faceted Crystal Shapes and their Transformation into Skeletons during Growth under Diffusion Control. *Crystallogr. Rev.* **4**, 3–71 (1994).

27. Mullins, W. W. & Sekerka, R. F. Morphological Stability of a Particle Growing by Diffusion or Heat Flow. *J. Appl. Phys.* **34**, 323–329 (1963).

28. Mullins, W. W. & Sekerka, R. F. Stability of a Planar Interface During Solidification of a Dilute Binary Alloy. *J. Appl. Phys.* **35**, 444–451 (1964).

29. Haxhimali, T., Karma, A., Gonzales, F. & Rappaz, M. Orientation selection in dendritic evolution. *Nat. Mater.* **5**, 660–664 (2006).

30. Yee, D. W., Lee, M. S., An, J. & Macfarlane, R. J. Reversible Diffusionless Phase Transitions in 3D Nanoparticle Superlattices. *J. Am. Chem. Soc.* **145**, 6051–6056 (2023).

31. Park, D. J. *et al.* Plasmonic photonic crystals realized through DNA-programmable assembly. *Proc. Natl. Acad. Sci. U.S.A.* **112**, 977–981 (2015).

32. Zornberg, L. Z. *et al.* Self-Assembling Systems for Optical Out-of-Plane Coupling Devices. *ACS Nano* **17**, 3394–3400 (2023).

33. Park, J. *et al.* Ultra-large-scale syntheses of monodisperse nanocrystals. *Nat. Mater.* **3**, 891–895 (2004).

Supplementary Files

This is a list of supplementary files associated with this preprint. Click to download.

- YeSINatureSynthesis2023.pdf